

# SIGMARK: SCALABLE IN-GENERATION WATERMARK WITH BLIND EXTRACTION FOR VIDEO DIFFUSION

Xinjie Zhu\*  
Lenovo Research, Beijing, China  
zhuxj11@lenovo.com

Zijing Zhao\*  
Lenovo Research, Beijing, China  
zhaozj23@lenovo.com

Hui Jin  
Lenovo Research, Beijing, China  
jinhui8@lenovo.com

Qingxiao Guo  
Lenovo Research, Beijing, China  
guoqx2@lenovo.com

Yilong Ma  
Lenovo Research, Beijing, China  
mayl9@lenovo.com

Yunhao Wang  
Lenovo Research, Beijing, China  
wangyh43@lenovo.com

Xiaobing Guo  
Lenovo Research, Beijing, China  
guoxba@lenovo.com

Weifeng Zhang<sup>†</sup>  
Lenovo Research, Beijing, China  
weifengz@lenovo.com

## ABSTRACT

Artificial Intelligence Generated Content (AIGC), particularly video generation with diffusion models, has been advanced rapidly. Invisible watermarking is a key technology for protecting AI-generated videos and tracing harmful content, and thus plays a crucial role in AI safety. Beyond post-processing watermarks which inevitably degrade video quality, recent studies have proposed distortion-free in-generation watermarking for video diffusion models. However, existing in-generation approaches are non-blind: they require maintaining all the message-key pairs and performing template-based matching during extraction, which incurs prohibitive computational costs at scale. Moreover, when applied to modern video diffusion models with causal 3D Variational Autoencoders (VAEs), their robustness against temporal disturbance becomes extremely weak. To overcome these challenges, we propose SIGMark, a Scalable In-Generation watermarking framework with blind extraction for video diffusion. To achieve blind-extraction, we propose to generate watermarked initial noise using a Global set of Frame-wise PseudoRandom Coding keys (GF-PRC), reducing the cost of storing large-scale information while preserving noise distribution and diversity for distortion-free watermarking. To enhance robustness, we further design a Segment Group-Ordering module (SGO) tailored to causal 3D VAEs, ensuring robust watermark inversion during extraction under temporal disturbance. Comprehensive experiments on modern diffusion models show that SIGMark achieves very high bit-accuracy during extraction under both temporal and spatial disturbances with minimal overhead, demonstrating its scalability and robustness. Our code is available at <https://github.com/JeremyZhao1998/SIGMark-release>.

## 1 INTRODUCTION

In the field of Artificial Intelligence Generated Content (AIGC), diffusion models have rapidly advanced image and video generation (Croitoru et al., 2023; Cao et al., 2024). Latent diffusion models proposed by Rombach et al. (2022) generates images by denoising sampled noise in latent space. Extending from this, video diffusion models generate temporally coherent frame sequences by enforcing both spatial and temporal consistency (Ho et al., 2022). With the rapid proliferation of AI-generated videos, privacy and security concerns have become increasingly critical (Wang et al., 2024). On the one hand, as a widely used creative tool, AI-generated high-quality videos constitute valuable intellectual property (IP) and necessitate reliable copyright identification. On the

\*Xinjie Zhu and Zijing Zhao contributed equally to this work.

<sup>†</sup>Corresponding author: Weifeng Zhang (weifengz@lenovo.com).

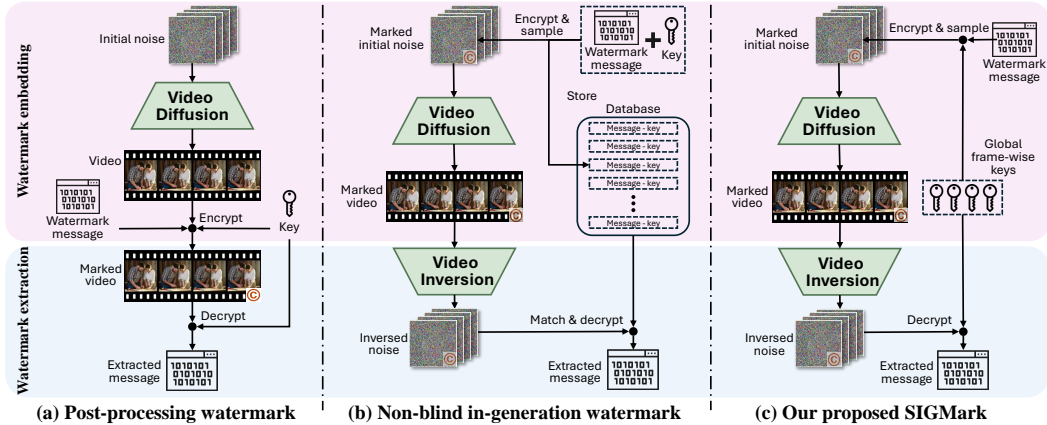


Figure 1: (a) Post-processing watermarks: embedding watermarks in pixel-space which inevitably degrades video quality. (b) Existing in-generation methods: maintaining all the message-key pairs for matching, incurring high extraction costs and poor robustness. (c) Our proposed SIGMark: a blind watermarking framework with global frame-wise PRC keys which is inherently scalable.

other hand, the ease of producing harmful or misleading content calls for strict control mechanisms, requiring effective methods to trace their source of generation.

To meet the demands of privacy and security, watermarking technology (Cox et al., 2007) has been widely applied in AIGC (Luo et al., 2025). Invisible watermarking embeds information in a way imperceptible to the human eye, thereby preserving visual quality while remaining robust to various distortions and even malicious attacks (Wang et al., 2023). For AI-generated videos, a straightforward approach is to treat them like conventional videos and apply invisible watermarking to each frame after generation (Luo et al., 2023; Zhang et al., 2024), known as post-processing watermarking (see Figure 1(a)). However, such methods inevitably introduce redundant information, thereby degrading overall video quality. Recently, in-generation watermarking has been explored for both image (Yang et al., 2024; Li et al., 2025) and video generation (Hu et al., 2025a;b). As illustrated in Figure 1(b), these methods embed watermark messages during generation process, typically by sampling a watermarked initial noise in which the message is encoded using a secret key. During extraction, the watermarked video is inverted (commonly via Denoising Diffusion Implicit Models (DDIM) inversion) back into latent noise, and then decoded with the key to recover the watermark. These approaches have been theoretically proven to be distortion-free for diffusion models.

Although in-generation video watermarking offers the advantage of being distortion-free, it still faces two critical challenges: (1) *High extraction cost at scale*. When extracting watermark messages from videos subject to temporal disturbances (e.g., frame removal during compression), current methods rely on template matching with the original latent noise. This requires maintaining all message-key pairs during watermark embedding, and computing matching functions across the entire database, as shown in Figure 1(b). Such approaches are non-blind, with the extraction cost growing linearly with the scale of users or generation requests, severely limiting scalability. (2) *Poor temporal robustness*. Modern video diffusion models (Yang et al., 2025; Kong et al., 2024) employ causal 3D Variational Autoencoders (VAE), which decode a group of adjacent frames from one temporal dimension of latent features. During extraction, video inversion requires the correct grouping of frames to reconstruct the latent feature. Temporal disturbance which disrupts the grouping will produce unrelated latent features, ultimately leading to very low extracted bit accuracy.

To address these issues and ensure usability at large-scale video generation platforms, we introduce SIGMark: scalable in-generation watermarking with blind extraction for video diffusion models.

To reduce the *high extraction cost at scale*, we propose Global Frame-wise PseudoRandom Coding (GF-PRC) scheme for watermark embedding, thereby enabling a blind watermarking framework. Specifically, a global set of frame-wise PRC keys (pseudorandom error-correction code by Christ & Gunn (2024)) is shared across all generation requests, with each key assigned to a group of temporal frames. Watermark messages are encoded into random latent noise with these keys, which preserves

diversity and generative performance. During extraction, the global frame-wise PRC directly decodes the inverted noise without matching with the original messages. Throughout this process, the system only needs to maintain the global frame-wise PRC keys, reducing extraction complexity from linear in the number of generation requests to constant, and achieving strong scalability.

To enhance *temporal robustness*, we introduce a Segment Group-Ordering (SGO) module tailored to causal 3D VAEs in modern video diffusion models. Specifically, for a video potentially affected by temporal disturbances, we first partition it into motion-consistent segments using Farneback optical flow; within each segment, a sliding-window grouping detector infers the original causal frame groups. This procedure recovers the correct grouping and, in turn, yields accurate inverted latents for watermark extraction under temporal disturbances.

We conduct comprehensive experiments on modern video diffusion models (HunyuanVideo by Kong et al. (2024) and Wan-2.2 by Wan et al. (2025)), covering both text-to-video (T2V) and image-to-video (I2V) pipelines. A subset of VBench-2.0 (Zheng et al., 2025) under 18 evaluation dimensions is sampled to generate 400 videos for evaluation. Results show that our method achieves very high bit accuracy with high watermark capacity with minimal extraction cost. Our method maintains high accuracy under spatial and temporal disturbances, demonstrating strong robustness. Our code is available at <https://github.com/JeremyZhao1998/SIGMark-release>.

In conclusion, the main contributions of this paper are:

- We identify two critical issues in existing in-generation video watermarks: high extraction cost and poor temporal robustness, which hinder their scalability to large platforms.
- We propose SIGMark, a scalable in-generation watermarking framework with blind extraction for video diffusion, effectively addressing the limitations of scalability and robustness.
- We conduct extensive experiments for SIGMark on modern video diffusion models and comprehensive evaluation benchmarks, demonstrating its effectiveness and robustness.

## 2 RELATED WORKS

### 2.1 DIFFUSION MODELS

In the field of Artificial Intelligence Generated Content (AIGC), diffusion models have rapidly advanced image and video generation. Latent diffusion model (LDM) (Rombach et al., 2022) synthesizes content by denoising sampled noise in latent space and decoding it through a Variational Autoencoder (VAE). Building on LDM, works such as SDXL (Podell et al., 2024), ControlNet (Zhang et al., 2023) and DiT (Peebles & Xie, 2023) further improve image generation with stronger photorealism and higher resolution, fine-grained structural control, and greater scalability. Extending from images, video diffusion models tackle the task of generating temporally coherent frame sequences (Ho et al., 2022). Following the success of Sora (OpenAI, 2024), a wave of open-source video diffusion models including KLING (Kuaishou Technology, 2024), HunyuanVideo (Kong et al., 2024), and Wan (Wan et al., 2025) has emerged. They adopt causal 3D VAEs that compress videos along spatial and temporal dimensions to form compact latent sequences for diffusion, enabling longer, higher-quality videos with improved temporal consistency. Our research focuses on watermarking for diffusion-generated videos and evaluates on HunyuanVideo and Wan-2.2.

### 2.2 VIDEO WATERMARKING

Video invisible watermarking embeds imperceptible, durable signals in video to enable rights management and piracy deterrence (Asikuzzaman & Pickering, 2017; Aberna & Agilandeswari, 2024). The straightforward image-based watermarking approaches operate frames individually (Hartung & Girod, 1998b; Hernandez et al., 2000), while video-based works explicitly exploit temporal information via compressed domain (Biswas et al., 2005; Noorkami & Mersereau, 2007) and motion vectors produced during compression (Mohaghegh & Fatemi, 2008). Recently, deep learning has been applied to watermarking for images (Zhu et al., 2018) and videos (Ben Jabra & Ben Farah, 2024): Zhang et al. (2019) introduced RivaGAN, training an encoder-decoder framework for robust watermarking. Subsequent work further advances robustness and capacity through curriculum learning (Ke et al., 2022), low-order recursive Zernike-moment embedding (He et al., 2023), multiscale

distribution modeling (Luo et al., 2023), complex wavelet transforms (Yasen et al., 2025; Huang et al., 2025), adversarially optimization under frequency domain Huang et al. (2024a), and spatiotemporal attention (Li et al., 2024; Yan et al., 2025). However, embedding extra signals inevitably degrades visual quality. We instead pursue in-generation watermarking for diffusion models, which is training-free and provably distortion-free.

### 2.3 IN-GENERATION WATERMARKING FOR DIFFUSION MODELS

With the rapid progress of image and video diffusion models, watermarking for diffusion-generated content has likewise gained traction. Recent work integrates watermark embedding into the generative process to reduce performance degradation. Fernandez et al. (2023) fine-tune the LDM decoder using a pre-trained watermark extractor, enabling reliable extraction from images produced by the fine-tuned model. Yang et al. (2024) introduce Gaussian Shading, the first approach to sample watermarked initial noise for image generation, which is provably distortion-free. Subsequent studies further enhance robustness during the embedding and inversion phases (Li et al., 2025; Fang et al., 2025). In-generation watermarking has also been extended from images to videos: Liu et al. (2025) propose a two-stage implanting scheme during the diffusion process. Other works encrypt the watermark message into the initial latent noise via Gaussian sampling (Hu et al., 2025a) or dynamic tree-ring (Zeng et al., 2025), preserving video generation quality. Hu et al. (2025b) adopt PRC for watermark encryption and decryption, maintaining generative diversity across messages. Despite being distortion-free, advanced in-generation methods by Hu et al. (2025a;b) still face high extraction costs at scale and poor temporal robustness. We are the first to identify and address these issues in modern video diffusion models, achieving strong scalability and temporal robustness.

## 3 METHOD

### 3.1 PROBLEM FORMULATION

This paper focuses on in-generation watermarking for video diffusion models. We first formalize the problem. Given a diffusion model  $\mathcal{M}$ , our goal is to embed a watermark message  $m$  into generated video frames  $\text{VF}(m) = \text{Embed}(\mathcal{M}; m)$  without degrading the performance of the diffusion model. The watermarked video frames may undergo temporal disturbances (e.g., frame drops) or spatial disturbances (e.g., cropping), yet the tampered frames  $\text{VF}'$  should still permit reliable watermark extraction. We adopt the blind-watermark setting: during extraction, neither the original message  $m$  nor the original generated video frames  $\text{VF}$  is available, and the message is recovered solely from the tampered video frames and the model, i.e.,  $\hat{m} = \text{Extract}(\mathcal{M}; \text{VF}')$ . We emphasize robustness: even under strong disturbances to  $\text{VF}'$ , the recovered message  $\hat{m}$  remains close to  $m$ .

During watermark embedding, we follow the in-generation scheme of Yang et al. (2024); Hu et al. (2025a). The watermark message  $m$  is encrypted into the initial latent noise without altering its distribution, i.e.,  $z_0(m) \sim \mathcal{N}(0, \mathbf{I})$ . The model then denoises this noise with text prompts to generate videos, thereby preserving generative performance. However, existing methods require the original message  $m$  for template matching during extraction, limiting scalability in real-world deployments. Moreover, when applied to modern diffusion models with causal 3D VAEs, they exhibit poor robustness under temporal disturbances.

### 3.2 FRAMEWORK OVERVIEW

An overview of our scalable in-generation watermarking framework, SIGMark, is shown in Figure 2. We follow the in-generation watermarking scheme which embeds the watermark message into the initial latent noise to generate distortion-free watermarked video through diffusion (left part of Figure 2), and then process the video through inversion to obtain inverted latent noise for watermark extraction (right part of Figure 2). To enable blind watermarking and reduce extraction cost at scale, we introduce a Global Frame-wise Pseudo-Random Coding (GF-PRC) scheme for message encryption and decryption. During embedding, the watermark message is encoded into the initial latent noise using a global set of frame-wise PRC keys, each key assigned to one temporal dimension of latent features. During extraction, given a possibly tampered video, a Segment Group-Ordering (SGO) module restores the correct causal frame grouping by Farneback optical flow segmentation

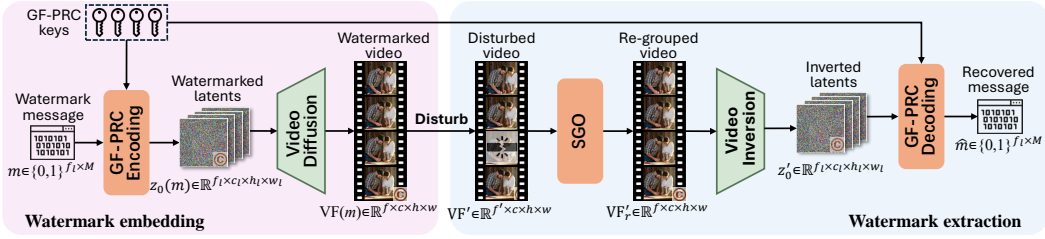


Figure 2: Overview of our proposed SIGMark. Embedding: We encode the watermark message into the initial latent noise using a Global set of Frame-wise Pseudo-Random Coding (GF-PRC) keys. The diffusion model then denoises this noise into video frames that carry the embedded messages. Extraction: A (possibly disturbed) video is first processed by our proposed Segment Group-Ordering (SGO) module to recover the correct causal frame grouping, then inverted to obtain the latent noise, from which the message is decoded using the GF-PRC keys. The system stores only the GF-PRC keys for both embedding and extraction, enabling blind watermarking.

and sliding-window grouping detector. We then perform inversion to recover the watermarked latent and decode the message with the GF-PRC keys. GF-PRC enables blind extraction where only the global keys are stored in the system, while maintaining high-accuracy message recovery under disturbances. We elaborate the details of our proposed modules in the following sections.

### 3.3 WATERMARK EMBEDDING

Following the in-generation watermarking scheme (Yang et al., 2024; Hu et al., 2025a), we map the watermark message bits into the initial latent noise without affecting the Gaussian distribution of the noise for watermark embedding. To achieve blind watermarking, we propose to utilize a Global set of Frame-wise Pseudo-Random coding (GF-PRC) scheme for watermark embedding.

#### 3.3.1 VIDEO GENERATION BY MODERN DIFFUSION MODELS

For a modern video diffusion model (Kong et al., 2024; Wan et al., 2025)  $\mathcal{M}$ , which consists of a text prompt encoder  $E_{\text{text}}$ , a denoising diffusion transformer  $T$ , and the encoder  $E_{3D}$  and decoder  $D_{3D}$  of the causal 3D Variational Autoencoders (VAE), the denoising steps happen on latent-space features  $z \in \mathbb{R}^{f_l \times c_l \times h_l \times w_l}$ , where  $f_l, c_l, h_l, w_l$  denote the frame, channel, height, and width dimensions in latent space. The diffusion transformer  $T$  denoises a randomly initialized latent noise  $z_0 \sim \mathcal{N}(o, \mathbf{I})$  guided by the text prompt:  $z_\tau = \text{Denoise}(T; z_0; E_{\text{text}}(\text{prompt}))$ , where  $\tau$  denotes the number of denoising steps. The denoised latent feature  $z_\tau$  is then processed by the causal 3D VAE decoder to generate video frames  $\text{VF} \in \mathbb{R}^{f \times c \times h \times w}$ , where  $f, c, h, w$  denote the frame, channel, height, and width of the generated video. The whole process can be formulated as:

$$\text{VF} = \text{Diffusion}(\mathcal{M}; z_0; \text{prompt}) \quad (1)$$

$$= D_{3D}(\text{Denoise}(T; z_0; E_{\text{text}}(\text{prompt}))). \quad (2)$$

The causal 3D VAE introduces information compression along both spatial and temporal dimensions, where  $f = f_l \times d_t$ ,  $h = h_l \times d_s$ , and  $w = w_l \times d_s$ , with  $d_t, d_s$  denoting the temporal and spatial compression ratios, respectively. As a result, a group of  $d_t$  frames is decoded from one temporal dimension of the latent features. Our proposed SIGMark embeds the watermark message into the latent noise via the GF-PRC scheme, yielding a sequence of watermark bits carried by a causal group of video frames, as detailed in the next paragraph.

#### 3.3.2 GLOBAL FRAME-WISE PSEUDORANDOM CODING SCHEME

We propose embedding all watermark messages using a global set of frame-wise pseudorandom coding keys, as shown in Figure 3. Specifically, for a watermark message  $m \in \{0, 1\}^{f_l \times M}$  where  $f_l$  is the number of latent frames and  $M$  is the bit length carried by each causal frame group, we encode  $m$  into a random template bit sequence  $\text{TP} \in \{0, 1\}^{f_l \times (c_l \times h_l \times w_l)}$  using the pseudorandom

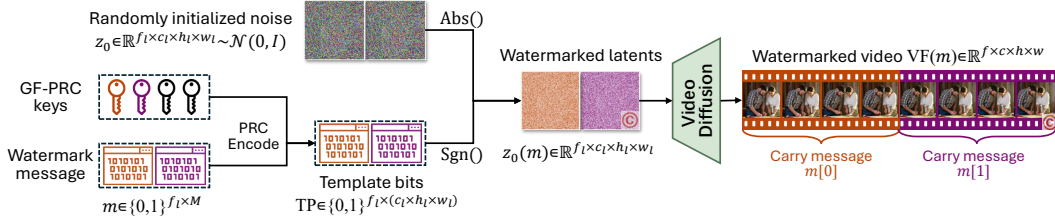


Figure 3: Watermark embedding with GF-PRC scheme. We set  $f_l = 2$ ,  $f = 8$  with compression ratio  $d_t = f/f_l = 4$  as an example. Orange and purple denote message  $m[0]$  and  $m[1]$  respectively.

error-correction code (simplified as pseudorandom code, PRC) proposed by Christ & Gunn (2024):

$$TP[i] = \text{PRC.Encode}(m[i]; K[i]), \quad i \in \{0, 1, 2, \dots, f_l - 1\} \quad (3)$$

Here,  $K$  denotes the pseudorandom error-correction coding keys;  $K[i]$  is the key for frame dimension  $i$  in latent space, with  $m[i] \in \{0, 1\}^M$  and  $TP[i] \in \{0, 1\}^{(c_l \times h_l \times w_l)}$ . We allocate one PRC key per causal frame group in latent space, enhancing robustness and enabling causal frame grouping and ordering information recovery (detailed in the next section). Given the randomized template TP, we map the watermark message into the initial latent noise by element-wise modulation:

$$z_0(m) = (TP * 2 - 1) * |z_0| \quad (4)$$

With the random absolute value from Gaussian sampling and the randomized template bits as the modulation signal, the embedded initial noise remains Gaussian,  $z_0(m) \sim \mathcal{N}(0, 1)$ , and thus does not degrade the diffusion model’s generative performance. Consequently, the generated video frames are watermarked with  $m$  via:

$$VF(m) = \text{Diffusion}(\mathcal{M}; z_0(m); \text{prompt}) \quad (5)$$

Note that in our GF-PRC scheme, the frame-wise PRC keys are global: every generation request shares the same key set, and each latent frame dimension carries one watermark sequence encoded by its corresponding PRC key. The total number of GF-PRC keys can be set to the maximum frame capacity of the video generation system, enabling watermarking for videos of arbitrary length. PRC by Christ & Gunn (2024) introduces a pseudo-random mapping that can encode even the same message into different random template bits, thereby preserving randomness in the initial latent noise under global keys, which traditional stream ciphers (e.g., ChaCha20(Bernstein et al., 2008)) used in prior in-generation non-blind methods(Yang et al., 2024; Hu et al., 2025a) cannot provide with the fixed keying material. The detailed explanation can be seen in Appendix A.

### 3.4 WATERMARK EXTRACTION

As shown in Figure 2, given a test video, we first apply the Segment Group-Ordering module to recover the grouping and ordering information of video frames, enhancing robustness against temporal disturbances, then perform diffusion-based inversion to obtain the inverted latent noise, and finally apply PRC decoding to recover the message.

#### 3.4.1 SEGMENT GROUP-ORDERING MODULE

A watermarked video may encounter various disturbances, among which temporal disturbances are particularly critical for modern diffusion models with causal 3D VAEs. As shown on the left of Figure 4, the original frames  $VF(m)$  are generated in causal groups of 4 (frames sharing the same color). After video clipping or frame drops, the disturbed video  $VF'$  loses both grouping and ordering information. If such frames are fed directly into the causal 3D VAE encoder, the mis-grouping (e.g., differently colored frames within a group) produces latent features that are inconsistent with those of  $VF(m)$ , thereby preventing reliable recovery of the message bits via inversion. To address the issue of weak temporal robustness, we propose a Segment Group-Ordering (SGO) module as shown in the right part of Figure 4 to recover the grouping and ordering information of the disturbed video for correct encoding.

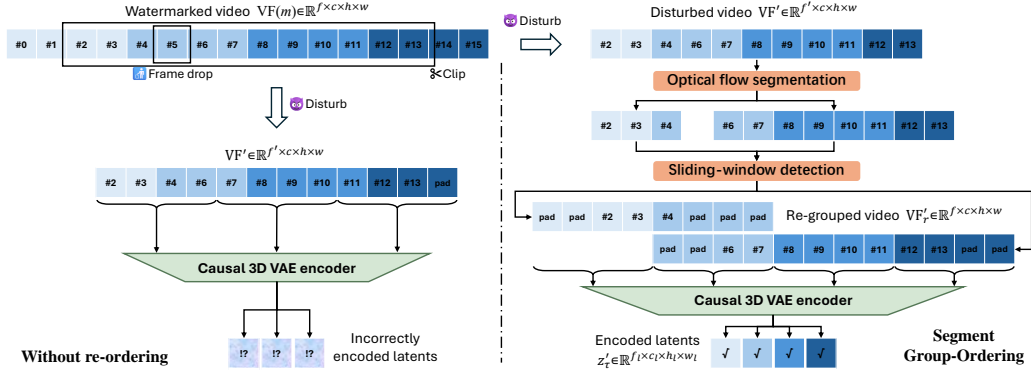


Figure 4: Segment Group-Ordering (SGO) module. We set compression ratio  $d_t = f/f_i = 4$  as an example. When temporal disturbances (e.g., clipping or frame drops) occur, the causal grouping is disrupted; without re-ordering, this leads to incorrectly encoded latent features. Our SGO module restores the correct grouping and ordering, yielding robust latent features for video inversion.

**Optical flow segmentation:** We propose an optical-flow method to partition a video into maximally contiguous subsequences with consistent temporal dynamics. For each adjacent pair  $(VF[t], VF[t+1])$ , we compute bidirectional Farneback flow and derive three indicators of temporal consistency: (i) median flow magnitude, (ii) forward-backward consistency, and (iii) motion-compensated residual. These are normalized via median absolute deviation and combined with a weighted sum to form a discontinuity score. The score is smoothed with a Gaussian filter, and temporal cut points are detected using hysteresis thresholding. The procedure runs near real time and outputs contiguous frame segments. Within each segment, we then perform sliding-window grouping detection. Further details of the optical-flow segmentation algorithm are provided in Appendix C.

**Sliding-window detection:** Given a contiguous frame segment, we only need to identify the first frame of a causal group, and the subsequent frames can then be grouped correctly. To this end, we leverage the global frame-wise PRC keys. Specifically, we pad  $(d_t - 1)$  frames at the beginning of the segment and apply a sliding window over the padded sequence. At sliding index  $j$ , we invert frames  $[j : j + 2 * d_t]$  to obtain two latent frame dimensions  $z'_0[j]$  and  $z'_0[j+1]$ . Using the global PRC keys, the frame index of each latent can be determined by:

$$\text{Idx}[\hat{j}] = \text{argmax}(\text{PRC.Detect}(z'_0[\hat{j}]; K[0, 1, \dots, f_l])), \text{Idx}[\hat{j}] \in \{0, 1, \dots, f_l\} \quad (6)$$

We stop sliding when the detections are consecutive, i.e.,  $\text{Idx}[\hat{j}] + 1 = \text{Idx}[\hat{j} + 1]$ , indicating that the current grouping yields the correct segment start for inversion. The results from all segments are then merged to produce the re-grouped frames  $VF'_r$ , as shown in Figure 4. Note that empty slots within each group are filled preferentially with available frames; any remaining slots are then padded. If an entire group contains no frames (caused by frame drop), we assign padding based on the nearest available frame. This procedure recovers correct ordering and grouping information and is robust to frame insertion, swapping, dropping, and clipping. Further details of the sliding-window detection algorithm are provided in Appendix C.

### 3.4.2 MESSAGE BITS EXTRACTION

Following the in-generation watermarking paradigm (Yang et al., 2024; Hu et al., 2025a), we perform inversion on the re-grouped frames to extract the watermark bits. The latent features  $z'_t \in \mathbb{R}^{f_i \times c_i \times h_i \times w_i}$  are first obtained via the causal 3D VAE encoder, and then inverted through the diffusion transformer (the flow-matching Euler discrete inversion for HunyuanVideo (Kong et al., 2024) and Wan (Wan et al., 2025)):

$$z'_\tau = E_{3D}(VF'_r) \quad (7)$$

$$z'_0 = \text{Inversion}(\mathcal{M}; z'_\tau; \text{prompt}_\emptyset) \quad (8)$$

where  $\text{prompt}_\emptyset$  denotes an empty prompt, since no original generation information is available. Given the inverted latent noise  $z'_0 \in \mathbb{R}^{f_i \times c_i \times h_i \times w_i}$ , we decode the GF-PRC keys  $K$  by applying

Table 1: Video watermarking results: message recovery bit accuracy and video quality score.<sup>1</sup>

Diffusion model		HunyuanVideo T2V				HunyuanVideo I2V			
Watermarking Method	Category	512 bits		512×16 bits		512 bits		512×16 bits	
		Bit acc↑	V-score↑	Bit acc↑	V-score↑	Bit acc↑	V-score↑	Bit acc↑	V-score↑
No-mark	–	–	0.490	–	0.490	–	0.463	–	0.463
DCT	Post	0.889	0.424	0.862	0.423	0.890	0.452	0.858	0.456
DT-CWT	Post	0.619	0.416	0.650	0.436	0.627	0.458	0.611	0.463
VideoMark	None-blind	0.873	0.507	0.758	0.502	0.846	0.483	0.707	0.482
VideoShield	None-blind	1.000	0.497	0.991	0.506	1.000	0.482	0.999	0.482
SIGMark(Ours)	Blind	0.958	0.506	0.885	0.499	0.981	0.472	0.905	0.488

PRC to the signs of  $z'_0$ :

$$\hat{m}[i] = \text{PRC.Decode} \left( \frac{\text{Sgn}(z'_0[i]) + 1}{2}; K[i] \right), \quad i \in \{0, 1, 2, \dots, f_l - 1\} \quad (9)$$

where  $\text{Sgn}(\cdot)$  is the sign function. With the global PRC key set, no additional information needs to be stored during generation, and no template matching (as in Hu et al. (2025a;b)) is required during extraction. Therefore, our proposed SIGMark enables blind watermarking with minor computation cost and strong scalability. Details of message extraction cost are provided in Appendix B.

## 4 EXPERIMENTS

In this section, we conduct experiments on modern video diffusion models. We detail the experimental setup in Section 4.1, report bit accuracy comparisons with existing methods in Section 4.2, assess temporal and spatial robustness in Section 4.3, conduct ablation studies in Section 4.4 and present evidence of scalability in Section 4.5.

### 4.1 EXPERIMENTAL SETTINGS

#### 4.1.1 DATASETS AND METRIC

To comprehensively assess modern video diffusion models, we conduct experiments on a subset of prompts from VBench-2.0(Zheng et al., 2025), which offers more evaluation dimensions and more complex prompts than VBench-1.0(Huang et al., 2024b) used by existing researches on earlier diffusion models(Hu et al., 2025a;b). Among the 18 dimensions in VBench-2.0, we select 3 prompts for the “diversity” dimension and generate 20 videos per prompt; for the remaining 17 dimensions, we select 5 prompts each and generate 4 videos per prompt, yielding a total of 400 videos. We report bit accuracy between the embedded message  $m$  and the recovered message  $\hat{m}$ . Video quality is evaluated using the VBench-2.0 protocols to obtain an overall quality score. Detailed examples of the constructed prompt set are provided in Appendix D.

#### 4.1.2 IMPLEMENTATION DETAILS

We evaluate on two open-source video diffusion models: HunyuanVideo(Kong et al., 2024) and Wan-2.2(Wan et al., 2025), both employing causal 3D VAEs with temporal and spatial compression ratios  $d_t = 4$  and  $d_s = 8$ . For each model, we consider both text-to-video (T2V) and image-to-video (I2V) tasks. For T2V, we generate videos at resolution  $h = 512$ ,  $w = 512$ , with 65 frames per video. The first frame is processed independently by the diffusion model, so no watermark is embedded in the first frame. The remaining  $f = 64$  frames form  $f_l = f/d_t = 16$  causal groups, for each group we maintain one frame-wise PRC key globally. For I2V, we use the same text prompt set to generate

<sup>1</sup>We implement DCT and DT-CWT through the open-source code of video-invisible-watermark and blind-video-watermark respectively, and we implement VideoMark and VideoShield by adapting their officially released code and hyper-parameter to new diffusion models and prompts.

Table 2: Watermark extraction bit accuracy under disturbances on HunyuanVideo I2V.

Method	Spatial disturbance				Temporal disturbance			
	w/o	G.noise	cmprs	blur	w/o	drop	insert	clip
VideoMark	0.85	0.64 <sub>↓0.21</sub>	0.63 <sub>↓0.22</sub>	0.64 <sub>↓0.21</sub>	0.71	0.52 <sub>↓0.19</sub>	0.51 <sub>↓0.20</sub>	0.51 <sub>↓0.20</sub>
VideoShield	1.00	1.00 <sub>↓0.00</sub>	0.99 <sub>↓0.01</sub>	1.00 <sub>↓0.00</sub>	0.99	0.89 <sub>↓0.10</sub>	0.84 <sub>↓0.15</sub>	0.83 <sub>↓0.16</sub>
SIGMark(Ours)	0.98	0.89 <sub>↓0.09</sub>	0.84 <sub>↓0.14</sub>	0.95 <sub>↓0.03</sub>	0.91	0.81 <sub>↓0.10</sub>	0.87 <sub>↓0.04</sub>	0.85 <sub>↓0.06</sub>

Table 3: Ablation study on our proposed modules on HunyuanVideo I2V

Method	Watermark embedding		Watermark extraction			
	Single PRC	GF-PRC(Ours)	w/o SGO	w/o OF-seg	w/o SW-det	SGO(Ours)
Bit acc	0.707	0.905	0.534	0.762	0.823	0.869

the initial image prompt by FLUX(Black Forest Labs et al., 2025) for evaluation. The generated image prompt examples are shown in Appendix D.

#### 4.2 WATERMARK EXTRACTION RESULTS

In this section, we compare our watermarking performance with existing approaches. As presented in Table 1, we report message bit accuracy (“Bit Acc”) and the VBench-2.0 score (“V-score”) for HunyuanVideo. Additional results for Wan-2.2 are provided in Appendix D. We consider two configurations: (1) embedding an identical 512-bit watermark message in every causal frame group of a video, and (2) embedding a distinct 512-bit watermark message per causal frame group, corresponding to total capacities of 512 bits and  $512 \times 16 = 8192$  bits per video, respectively.

We compare our method against four baselines: DCT(Hartung & Girod, 1998a), DT-CWT(Coria et al., 2008), VideoShield(Hu et al., 2025a), and VideoMark(Hu et al., 2025b). DCT and DT-CWT are widely used post-processing watermarking methods for general videos, whereas VideoShield and VideoMark are recent in-generation methods for video diffusion models but are non-blind. For post-processing methods, we first generate a set of standard videos with the diffusion model and then apply watermarking of different settings. As shown in Table 1, post-processing watermarking causes notable quality degradation relative to no-watermark videos, while in-generation methods leave visual quality essentially unaffected. Our proposed SIGMark can be proved to be performance-lossless. Detailed proof can be found in Appendix A. Our proposed SIGMark with blind extraction attains very high bit accuracy under both lower and higher capacity settings, surpassing VideoMark by large margins and remaining competitive with VideoShield which requires access to the original watermark information, thereby demonstrating the effectiveness of our approach.

#### 4.3 ROBUSTNESS

We assess the robustness of watermarking methods under both spatial and temporal perturbations in Table 2. We apply spatial disturbance under 512 bits watermark and temporal disturbances under  $512 \times 16$  bits. “w/o” denotes without disturbance. “G.noise”, “cmprs” and “blur” denotes Gaussian noise, mpeg compression and blurring, respectively. In temporal disturbances, we randomly drop, insert or clip out 30 frames. The performance degradation compared with no disturbances is marked as subscript. For spatial disturbances, our approach incurs only marginal performance degradation, particularly when compared to VideoMark. Under the challenging temporal disturbances, VideoMark and VideoShield suffer substantial degradation on diffusion models with causal 3D VAEs, primarily due to incorrect grouping of causal frame groups. Our method mitigates this issue, achieving negligible performance loss and thereby improving temporal robustness. It is worth noting that our method does not attain 100% bit accuracy. We attribute this to the relationship of error-tolerance characteristics of PRC coding and the accuracy of diffusion inversion for different models. A detailed analysis of PRC coding robustness is provided in Appendix E.

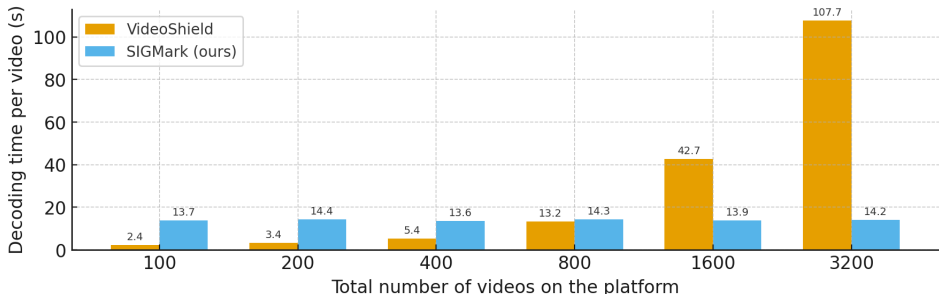


Figure 5: The decoding time cost during watermark extraction.

#### 4.4 ABLATION STUDIES

We conduct ablation studies to evaluate the contribution of each proposed component in Table 3. “OF-seg” and “SW-det” denotes optical flow segmentation and sliding window detection, respectively. For the ablation study of watermark embedding modules, we evaluate a 512×16-bit watermark on generated videos without disturbances. For the ablation study of watermark extraction modules, we evaluate a 512×16-bit watermark under temporal disturbance by inserting 30 random frames. When SGO and OF-seg are removed, we simply truncate the video to the target length. When SW-det is removed, we perform PRC detection by assuming that each segment starts at the beginning of a frame group. For the GF-PRC scheme, removing it reduces our method to the same coding strategy as VideoMark, which exhibits limited bit accuracy under the blind setting without template matching. In contrast, GF-PRC not only enables blind extraction but also improves bit accuracy by introducing inter-frame redundant error tolerance. For the SGO module, both optical-flow-based segmentation and sliding-window detection are critical for recovering frame grouping and ordering; omitting either component leads to a noticeable accuracy drop.

#### 4.5 EVIDENCE OF SCALABILITY

Baseline methods such as VideoShield and VideoMark are non-blind watermarking schemes: they require storing all watermark-related information (messages, encoding keys, etc.) during generation and matching against all stored information during extraction. Therefore, extraction cost grows with the total number of generated videos. Our method, SIGMark, is blind: it maintains only a global set of frame-wise PRC keys and does not require any sample-specific metadata during extraction. As a result, it supports large-scale video generation platforms with constant extraction cost. We analyze extraction time cost under scenarios where the total number of videos generated by the platform varies. Experiments are conducted under HunyuanVideo I2V with 512x16-bit watermark without disturbances. For fairness, we run inversion on GPU, and all remaining extraction steps including decryption and message matching on CPU. As shown in Figure 5, the results demonstrate that the time cost of VideoShield scales linearly with the number of generated videos, which becomes impractical as the platform scales to millions of videos. In contrast, SIGMark remains constant, demonstrating strong scalability.

## 5 CONCLUSION

Watermarking for video diffusion models is critical for ensuring safety and privacy control in AIGC. In this work, we introduce SIGMark, the first blind in-generation video watermarking method for modern diffusion models, offering strong scalability and practical applicability. To enable blind extraction without storing large-scale watermarking references, we propose a Global Frame-wise Pseudo-Random Code (GF-PRC) scheme, which encodes watermark messages into the initial latent noise without compromising video quality or diversity. To further enhance temporal robustness, we design a Segment Group-Ordering (SGO) module tailored for causal 3D VAEs, ensuring correct watermark inversion. Extensive experiments demonstrate that our approach achieves high bit accuracy with minimal overhead, validating its scalability and robustness.

## REFERENCES

- P Aberna and Loganathan Agilandeewari. Digital image and video watermarking: methodologies, attacks, applications, and future directions. *Multimedia Tools and Applications*, 83(2):5531–5591, 2024.
- Md Asikuzzaman and Mark R Pickering. An overview of digital video watermarking. *IEEE Transactions on Circuits and Systems for Video Technology*, 28(9):2131–2153, 2017.
- Saoussen Ben Jabra and Mohamed Ben Farah. Deep learning-based watermarking techniques challenges: a review of current and future trends. *Circuits, Systems, and Signal Processing*, 43(7):4339–4368, 2024.
- Daniel J Bernstein et al. Chacha, a variant of salsa20. In *Workshop record of SASC*, volume 8, pp. 3–5. Lausanne, Switzerland, 2008.
- Satyendra Biswas, Sunil R Das, and Emil M Petriu. An adaptive compressed mpeg-2 video watermarking scheme. *IEEE transactions on Instrumentation and Measurement*, 54(5):1853–1861, 2005.
- Black Forest Labs et al. Flux.1 kontext: Flow matching for in-context image generation and editing in latent space, 2025. arXiv preprint arXiv:2506.15742.
- Hanqun Cao, Cheng Tan, Zhangyang Gao, Yilun Xu, Guangyong Chen, Pheng-Ann Heng, and Stan Z Li. A survey on generative diffusion models. *IEEE transactions on knowledge and data engineering*, 36(7):2814–2830, 2024.
- Miranda Christ and Sam Gunn. Pseudorandom error-correcting codes. In *Annual International Cryptology Conference*, pp. 325–347. Springer, 2024.
- Lino E. Coria, Mark R. Pickering, and Panos Nasiopoulos. A video watermarking scheme based on the dual-tree complex wavelet transform. *IEEE Transactions on Information Forensics and Security*, 3(3):466–474, 2008. doi: 10.1109/TIFS.2008.927421.
- Ingemar J. Cox, Matthew L. Miller, Jeffrey A. Bloom, Jessica Fridrich, and Ton Kalker. *Digital Watermarking and Steganography*. Morgan Kaufmann, 2007.
- Florinel-Alin Croitoru, Vlad Hondru, Radu Tudor Ionescu, and Mubarak Shah. Diffusion models in vision: A survey. *IEEE transactions on pattern analysis and machine intelligence*, 45(9):10850–10869, 2023.
- Han Fang, Kejiang Chen, Zijin Yang, Bosen Cui, Weiming Zhang, and Ee-Chien Chang. Cosda: Enhancing the robustness of inversion-based generative image watermarking framework. In *Proceedings of the AAAI Conference on Artificial Intelligence*, volume 39, pp. 2888–2896, 2025.
- Pierre Fernandez, Guillaume Couairon, Hervé Jégou, Matthijs Douze, and Teddy Furon. The stable signature: Rooting watermarks in latent diffusion models. In *Proceedings of the IEEE/CVF International Conference on Computer Vision*, pp. 22466–22477, 2023.
- Frank Hartung and Bernd Girod. Watermarking of uncompressed and compressed video. *Signal Processing*, 66(3):283–301, 1998a. doi: 10.1016/S0165-1684(98)00011-5.
- Frank Hartung and Bernd Girod. Watermarking of uncompressed and compressed video. *Signal processing*, 66(3):283–301, 1998b.
- Mingze He, Hongxia Wang, Fei Zhang, Sani M. Abdullahi, and Ling Yang. Robust blind video watermarking against geometric deformations and online video sharing platform processing. *IEEE Transactions on Dependable and Secure Computing*, 20(6):4702–4718, 2023. doi: 10.1109/TDSC.2022.3232484.
- Juan R Hernandez, Martin Amado, and Fernando Perez-Gonzalez. Dct-domain watermarking techniques for still images: Detector performance analysis and a new structure. *IEEE transactions on image processing*, 9(1):55–68, 2000.

- Jonathan Ho, Tim Salimans, Alexey Gritsenko, William Chan, Mohammad Norouzi, and David J Fleet. Video diffusion models. *Advances in neural information processing systems*, 35:8633–8646, 2022.
- Runyi Hu, Jie Zhang, Yiming Li, Jiwei Li, Qing Guo, Han Qiu, and Tianwei Zhang. Videoshield: Regulating diffusion-based video generation models via watermarking. In *Proceedings of the Thirteenth International Conference on Learning Representations*, 2025a. URL <https://openreview.net/forum?id=uzz3qAYy0D>.
- Xuming Hu, Hanqian Li, Jungang Li, and Aiwei Liu. Videomark: A distortion-free robust watermarking framework for video diffusion models, 2025b.
- Huayang Huang, Yu Wu, and Qian Wang. Robin: Robust and invisible watermarks for diffusion models with adversarial optimization. *Advances in Neural Information Processing Systems*, 37:3937–3963, 2024a.
- I.-Chun Huang, Ji-Yan Wu, and Wei Tsang Ooi. Rbmark: Robust and blind video watermark in dt cwt domain. *Journal of Visual Communication and Image Representation*, 109:104438, 2025. ISSN 1047-3203. doi: <https://doi.org/10.1016/j.jvcir.2025.104438>. URL <https://www.sciencedirect.com/science/article/pii/S1047320325000525>.
- Ziqi Huang, Yinan He, Jiashuo Yu, Fan Zhang, Chenyang Si, Yuming Jiang, Yuanhan Zhang, Tianxing Wu, Qingyang Jin, Nattapol Chanpaisit, Yaohui Wang, Xinyuan Chen, Limin Wang, Dahua Lin, Yu Qiao, and Ziwei Liu. VBench: Comprehensive benchmark suite for video generative models. In *Proceedings of the IEEE/CVF Conference on Computer Vision and Pattern Recognition*, 2024b.
- Zehui Ke, Hailiang Huang, Yingwei Liang, Yi Ding, Xin Cheng, and Qingyao Wu. Robust video watermarking based on deep neural network and curriculum learning. In *2022 IEEE International Conference on e-Business Engineering (ICEBE)*, pp. 80–85, 2022. doi: 10.1109/ICEBE55470.2022.00023.
- Weijie Kong, Qi Tian, Zijian Zhang, Rox Min, Zuozhuo Dai, Jin Zhou, Jiangfeng Xiong, Xin Li, Bo Wu, Jianwei Zhang, et al. Hunyuanvideo: A systematic framework for large video generative models, 2024.
- Kuaishou Technology. Kuaishou unveils proprietary video generation model ‘kling’, 2024. URL <https://ir.kuaishou.com/node/9646/pdf>. Press release.
- Jian Li, Tao Zuo, Bin Ma, Chunpeng Wang, Peng Zhang, Huanhuan Zhao, and Zhengzhong Zhao. Robust video watermarking network based on channel spatial attention. In *2024 International Joint Conference on Neural Networks (IJCNN)*, pp. 1–8, 2024. doi: 10.1109/IJCNN60899.2024.10650701.
- Kecen Li, Zhicong Huang, Xinwen Hou, and Cheng Hong. Gaussmarker: Robust dual-domain watermark for diffusion models. In *The Forty-Second International Conference on Machine Learning*, 2025. URL <https://openreview.net/forum?id=m7Mx14cxv8>.
- Xiaohang Liu, Heng Chang, Jinfu Wei, Lei Zhu, Li Liu, Likun Li, Shiji Zhou, Chengyuan Li, Di Xu, and Wei Gao. Implanting robust watermarks in latent diffusion models for video generation. In *ICASSP 2025 - 2025 IEEE International Conference on Acoustics, Speech and Signal Processing (ICASSP)*, pp. 1–5, 2025. doi: 10.1109/ICASSP49660.2025.10888991.
- Huixin Luo, Li Li, and Juncheng Li. Digital watermarking technology for ai-generated images: A survey. *Mathematics*, 13(4):651, 2025. doi: 10.3390/math13040651.
- Xiyang Luo, Yinxiao Li, Huiwen Chang, Ce Liu, Peyman Milanfar, and Feng Yang. Dvmark: A deep multiscale framework for video watermarking. *IEEE Transactions on Image Processing*, 32:4371–4385, 2023. doi: 10.1109/TIP.2023.3251737.
- Najla Mohaghegh and Omid Fatemi. H. 264 copyright protection with motion vector watermarking. In *2008 International Conference on Audio, Language and Image Processing*, pp. 1384–1389. IEEE, 2008.

- Maneli Noorkami and Russell M Mersereau. A framework for robust watermarking of h. 264-encoded video with controllable detection performance. *IEEE Transactions on information forensics and security*, 2(1):14–23, 2007.
- OpenAI. Video generation models as world simulators, 2024. URL <https://openai.com/index/video-generation-models-as-world-simulators/>. Official model announcement and technical overview.
- William Peebles and Saining Xie. Scalable diffusion models with transformers. In *Proceedings of the IEEE/CVF international conference on computer vision*, pp. 4195–4205, 2023.
- Dustin Podell, Zion English, Kyle Lacey, Andreas Blattmann, Tim Dockhorn, Jonas Müller, Joe Penna, and Robin Rombach. Sdxl: Improving latent diffusion models for high-resolution image synthesis. In *Proceedings of the International Conference on Learning Representations (ICLR)*. OpenReview.net, 2024. URL <https://openreview.net/forum?id=di52zR8xgf>. Spotlight.
- Robin Rombach, Andreas Blattmann, Dominik Lorenz, Patrick Esser, and Björn Ommer. High-resolution image synthesis with latent diffusion models. In *Proceedings of the IEEE/CVF Conference on Computer Vision and Pattern Recognition*, pp. 10684–10695, 2022.
- Team Wan, Ang Wang, Baole Ai, Bin Wen, Chaojie Mao, Chen-Wei Xie, Di Chen, Feiwu Yu, Haiming Zhao, Jianxiao Yang, et al. Wan: Open and advanced large-scale video generative models, 2025.
- Tao Wang, Yushu Zhang, Shuren Qi, Ruoyu Zhao, Zhihua Xia, and Jian Weng. Security and privacy on generative data in aigc: A survey. *ACM Computing Surveys*, 57(4), 2024. doi: 10.1145/3703626.
- Zihan Wang, Olivia Byrnes, Hu Wang, Ruoxi Sun, Congbo Ma, Huaming Chen, Qi Wu, and Minhui Xue. Data hiding with deep learning: A survey unifying digital watermarking and steganography. *IEEE Transactions on Computational Social Systems*, 10(6):2985–2999, 2023. doi: 10.1109/TCSS.2023.3268950.
- Quan Yan, Yuanjing Luo, Zhangdong Wang, Junhua Xi, Geming Xia, and Zhiping Cai. Spatiotemporal attention-based real-time video watermarking. *Data Mining and Knowledge Discovery*, 39(5):62, 2025.
- Zhuoyi Yang, Jiayan Teng, Wendi Zheng, Ming Ding, Shiyu Huang, Jiazheng Xu, Yuanming Yang, Wenyi Hong, Xiaohan Zhang, Guanyu Feng, Da Yin, Yuxuan Zhang, Weihang Wang, Yean Cheng, Bin Xu, Xiaotao Gu, Yuxiao Dong, and Jie Tang. Cogvideox: Text-to-video diffusion models with an expert transformer. In *Proceedings of the Thirteenth International Conference on Learning Representations*, 2025. URL <https://arxiv.org/abs/2408.06072>.
- Zijin Yang, Kai Zeng, Kejiang Chen, Han Fang, Weiming Zhang, and Nenghai Yu. Gaussian shading: Provable performance-lossless image watermarking for diffusion models. In *Proceedings of the IEEE/CVF Conference on Computer Vision and Pattern Recognition (CVPR)*, pp. 12162–12171, June 2024.
- Kamil Yasen, Guiquan Wan, Li Zhan, Ke Qin, and Ye Li. Dtcwt-based video watermarking robust to recompression attack. In Guangqiang Yin, Xiaodong Liu, Jian Su, and Yangzhao Yang (eds.), *Proceedings of the 14th International Conference on Computer Engineering and Networks*, pp. 177–188, Singapore, 2025. Springer Nature Singapore. ISBN 978-981-96-4229-8.
- Shunyang Zeng, Linlin Yang, Jin Yang, Yezhen Wang, and Tianyu Gao. Dtr: Dynamic tree-ring watermarking framework for diffusion-based video generation. In *ICASSP 2025 - 2025 IEEE International Conference on Acoustics, Speech and Signal Processing (ICASSP)*, pp. 1–5, 2025. doi: 10.1109/ICASSP49660.2025.10888152.
- Kevin Alex Zhang, Lei Xu, Alfredo Cuesta-Infante, and Kalyan Veeramachaneni. Robust invisible video watermarking with attention. *arXiv preprint arXiv:1909.01285*, 2019.

Lvmin Zhang, Anyi Rao, and Maneesh Agrawala. Adding conditional control to text-to-image diffusion models. In *Proceedings of the IEEE/CVF international conference on computer vision*, pp. 3836–3847, 2023.

Zhiwei Zhang, Han Wang, Guisong Wang, and Xinxiao Wu. Hide and track: Towards blind video watermarking network in frequency domain. *Neurocomputing*, 579:Article 127435, 2024. doi: 10.1016/j.neucom.2024.127435.

Dian Zheng, Ziqi Huang, Hongbo Liu, Kai Zou, Yinan He, Fan Zhang, Lulu Gu, Yuanhan Zhang, Jingwen He, Wei-Shi Zheng, Yu Qiao, and Ziwei Liu. Vbench-2.0: Advancing video generation benchmark suite for intrinsic faithfulness, 2025.

Jiren Zhu, Russell Kaplan, Justin Johnson, and Li Fei-Fei. Hidden: Hiding data with deep networks. In *Proceedings of the European conference on computer vision (ECCV)*, pp. 657–672, 2018.

# SUPPLEMENTARY MATERIAL OF SIGMARK: SCALABLE IN-GENERATION WATERMARK WITH BLIND EXTRACTION FOR VIDEO DIFFUSION

Xinjie Zhu\*

Lenovo Research, Beijing, China  
zhuxj11@lenovo.com

Zijing Zhao\*

Lenovo Research, Beijing, China  
zhaozj23@lenovo.com

Hui Jin

Lenovo Research, Beijing, China  
jinhui8@lenovo.com

Qingxiao Guo

Lenovo Research, Beijing, China  
guoqx2@lenovo.com

Yilong Ma

Lenovo Research, Beijing, China  
may19@lenovo.com

Yunhao Wang

Lenovo Research, Beijing, China  
wangyh43@lenovo.com

Xiaobing Guo

Lenovo Research, Beijing, China  
guoxba@lenovo.com

Weifeng Zhang<sup>†</sup>

Lenovo Research, Beijing, China  
weifengz@lenovo.com

In this material, we include the following contents as supplements of our paper: (1) an explanation of our performance-lossless watermarking in Section A; (2) an analysis of the computational overhead of our method in Section B, demonstrating the scalability of SIGMark; (3) detailed implementation of the proposed Segment Group-Ordering (SGO) module in Section C; (4) additional experimental details and results on video watermarking in Section D; (5) an analysis of the performance bottlenecks of our method, outlining future research directions in Section E; (6) a statement on the usage of Large Language Models (LLMs) in this paper in Section F.

## A IMPACT OF WATERMARKING ON VIDEO DIFFUSION SYSTEMS

### A.1 STREAM CIPHER UNAVAILABLE FOR BLIND WATERMARKING

To embed a watermark message into the video diffusion model’s initial latent noise while remaining performance-lossless, the message must be encoded via a cryptographic (pseudo) randomized encoder so that the induced perturbations are statistically indistinguishable from natural noise. Stream ciphers such as ChaCha20 (Bernstein et al., 2008) can produce pseudorandom code streams and offer good noise resilience. However, their keystreams are deterministic given a fixed key (and nonce). Consequently, if a global key is reused and the message is fixed, the resulting codeword is also fixed, which harms generative diversity by mapping identical messages to identical latent sign patterns across runs. Preserving diversity would require a fresh per-generation secret (e.g., a new key/nonce) and thus auxiliary side information for extraction, rendering such schemes inherently none-blind and imposing substantial storage and coordination overhead at scale (tracking a large number of key-message pairs). Similar conclusion has been stated by Thietke et al. (2025). In contrast, our approach targets blind watermarking with a single or a set of global keys by adopting a PRC (Pseudorandom error-correction Code proposed by Christ & Gunn (2024)) that is explicitly randomized at encoding time: the same message admits many codewords drawn from a pseudorandom ensemble. This probabilistic encoding preserves sample diversity across generations without storing per-instance secrets, while still enabling blind extraction under global keys.

### A.2 PROOF OF OUR PROPOSED METHOD BEING PERFORMANCE-LOSSLESS

Prior works often observe that inserting watermark embedding modules degrades model performance when evaluated by metrics such as Peak Signal-to-Noise Ratio (PSNR) and Fréchet Inception Distance (FID), which are more suitable for post-processing methods. To assess methods that inte-

\*Xinjie Zhu and Zijing Zhao contributed equally to this work.

<sup>†</sup>Corresponding author: Weifeng Zhang (weifengz@lenovo.com).

grate watermark embedding within the video generation process, we adopt a complexity-theoretic indistinguishability notion (inspired by cryptographic security definitions) to characterize the impact of watermarking on model performance. Concretely, consider a probabilistic game between a watermarked video  $\text{VF}(m)$  and a normally generated video  $\text{VF}$ .

The watermarking method is *performance-lossless* if, for any probabilistic polynomial-time (PPT) tester (distinguisher)  $A$ , it holds that

$$|\Pr[A(\text{VF}(m)) = 1] - \Pr[A(\text{VF}) = 1]| < \text{negl}(\rho), \quad (10)$$

where  $\rho$  is the security parameter (e.g., the length of the PRC keys  $K$ ), and  $\text{negl}(\rho)$  denotes a function negligible in  $\rho$  (i.e., smaller than the inverse of any polynomial in  $\rho$ ).

We prove the claim by contradiction. Assume that  $\text{VF}(m)$  and  $\text{VF}$  are distinguishable by some PPT tester  $A$  with non-negligible advantage  $\delta > 0$ :

$$|\Pr[A(\text{VF}(m)) = 1] - \Pr[A(\text{VF}) = 1]| = \delta. \quad (11)$$

Let the entire video generation pipeline, comprising the diffusion transformer  $T_{\text{diff}}$  and the causal 3D VAE decoder  $D_{3D}$ , start from an initial latent noise  $z_0^{(\cdot)}$ . Substituting the generative process into (11) yields

$$|\Pr[A(D_{3D}(T_{\text{diff}}(z_0(m)))) = 1] - \Pr[A(D_{3D}(T_{\text{diff}}(z_0)) = 1)] = \delta, \quad (12)$$

where  $z_0(m)$  denotes the initial latent noise whose sign pattern is determined by the message  $m$  via our PRC encoding with keys  $K$  (hence forming a pseudorandom sign sequence), and  $z_0$  denotes the initial noise used for standard generation, drawn from a truly random distribution (e.g.,  $z_0 \sim \mathcal{N}(0, \mathbf{I})$ ).

Since  $D_{3D}$  and  $T_{\text{diff}}$  are deterministic PPT algorithms, they can be treated as subroutines available to the tester. Define a new tester  $A_{\text{gen}} = A \circ D_{3D} \circ T_{\text{diff}}$ . Then (12) reduces to distinguishing the initial latents:

$$|\Pr[A_{\text{gen}}(z_0(m)) = 1] - \Pr[A_{\text{gen}}(z_0) = 1]| = \delta. \quad (13)$$

Equation (13) asserts that a PPT algorithm can distinguish a latent tensor with a pseudorandom sign pattern ( $z_0(m)$ ) from one with truly random signs ( $z_0$ ) with non-negligible advantage.

However, our PRC mechanism is built upon cryptographic principles: the global keys  $K$  are generated via a secure pseudorandom function (PRF). A fundamental property of a secure PRF is that its output is computationally indistinguishable from uniform randomness; consequently, the sign patterns produced by  $\text{PRC.Encode}(K, m)$  are computationally indistinguishable from truly random signs. This contradicts (13), which would enable distinguishing PRC-generated signs from random in PPT, violating the PRF security assumption.

Therefore, the assumption in (11) is false. It follows that no PPT tester can distinguish watermarked videos from normally generated videos with non-negligible advantage, and thus our video watermarking method is performance-lossless under the above complexity-theoretic definition.

## B COMPUTATION OVERHEAD

### B.1 COMPUTATION COMPLEXITY ANALYSIS

Consider a large-scale video generation platform based on video diffusion models. We analyze the computational complexity of watermark embedding and extraction for our method and existing in-generation watermarking approaches (Hu et al., 2025a;b). Let  $f$  denote the maximum number of frames per video,  $h \times w$  the spatial resolution,  $t_{\text{diff}}$  the time for denoising or inversion (correlated with  $f \times h \times w$ ),  $M$  the watermark message length,  $K$  the key length, and  $t_{\text{encrypt}}$  the encryption/decryption time (correlated with  $M$  and  $f \times h \times w$ ). Let  $N$  denote the number of videos or generation requests in the system.

For in-generation watermarking, the embedding process incurs no additional spatial cost beyond video generation, and the temporal cost is a single encryption step  $t_{\text{encrypt}}$ , giving a total cost of:  $t_{\text{encrypt}} + t_{\text{diff}}$ . However, non-blind watermarking requires storing key-message or key-template pairs for extraction, resulting in an additional spatial cost of:  $O(N \times (M + K))$ . For our proposed

blind watermarking, only global frame-wise keys are maintained, with spatial cost:  $O(f \times K)$ . For extraction, non-blind watermarking requires matching against all stored watermark information. Under temporal disturbances, matching must be performed between watermark template bits for every frame, leading to a temporal complexity of:  $O(N \times f \times f \times M)$ , and a total complexity of:  $O(N \times f^2 \times M) + t_{\text{diff}} + t_{\text{decrypt}}$ . In contrast, our proposed SIGMark compares inverted latents with all frame-wise keys, yielding a total cost of:  $t_{\text{diff}} + f \times t_{\text{decrypt}}$ .

In typical experiments where  $N$ ,  $M$ , and  $f$  are of the same order, the dominant cost is  $t_{\text{diff}}$ . However, in large-scale systems where  $N \gg f$ , the parameters  $f, h, w, M, K$  can be treated as constants (e.g.,  $f = 64, h = w = 512, M = 512$ , while  $N \sim 10^8$ ). In this setting, the  $O(N)$  spatial and temporal cost of non-blind watermarking becomes prohibitive, whereas our proposed SIGMark maintains constant complexity, demonstrating strong scalability.

## B.2 EXPERIMENTED COMPUTATION TIME AND MEMORY USAGE ON HARDWARE

All experiments are conducted on NVIDIA A800 GPUs with `bfloat16` precision. On Hunyuan-Video, generating a single video with  $f = 65, h = 512$ , and  $w = 512$  takes approximately 4 minutes, with watermark embedding time being negligible. Processing the dataset of 400 videos requires about 1600 A800 GPU hours. For watermark extraction, PRC detection and decoding take roughly 30 seconds per sample on CPU, which can potentially be optimized through parallelization. Notably, this computation time remains constant regardless of the scale of video generation.

## C DETAILED IMPLEMENTATION OF SGO

### C.1 DETAILED IMPLEMENTATION OF OPTICAL FLOW SEGMENTATION

We aim to partition a sequence of frames  $\{I_t\}_{t=0}^{n-1}$  into contiguous segments that are likely temporally consistent, even under frame deletions, insertions, or swaps. For pre-processing, each frame is converted to grayscale and downsampled so that its short side does not exceed a fixed size (default 288), reducing computational cost without introducing upsampling artifacts. For Optical Flow Estimation, for each adjacent pair  $(I_t, I_{t+1})$ , we compute forward and backward Farneback optical flow fields, denoted as  $\mathbf{F}^{t \rightarrow t+1}$  and  $\mathbf{F}^{t+1 \rightarrow t}$ . We then calculate boundary features. For each boundary  $t|t+1$ , we compute four robust signals:

$$M_t = \text{median}_{\mathbf{x}} \|\mathbf{F}^{t \rightarrow t+1}(\mathbf{x})\|_2, \quad (14)$$

$$C_t = \text{median}_{\mathbf{x}} \|\mathbf{F}^{t \rightarrow t+1}(\mathbf{x}) + \mathbf{F}^{t+1 \rightarrow t}(\mathbf{x} + \mathbf{F}^{t \rightarrow t+1}(\mathbf{x}))\|_2, \quad (15)$$

$$R_t = \frac{1}{255|\Omega|} \sum_{\mathbf{x} \in \Omega} |\hat{I}_{t \rightarrow t+1}(\mathbf{x}) - I_{t+1}(\mathbf{x})|, \quad (16)$$

$$\Delta M_t = \begin{cases} 0, & t = 0, \\ |M_t - M_{t-1}|, & t \geq 1. \end{cases} \quad (17)$$

Here,  $M_t$  is the median flow magnitude,  $C_t$  measures forward-backward consistency,  $R_t$  is the motion-compensated residual after warping  $I_t$  to  $I_{t+1}$  using backward flow, and  $\Delta M_t$  captures speed changes. Each signal is standardized using a robust Z-score based on the median absolute deviation (MAD):

$$z(x) = 0.6745 \cdot \frac{x - \text{median}(x)}{\text{MAD}(x) + 10^{-9}}. \quad (18)$$

The final discontinuity score for boundary  $t$  is a weighted combination:

$$\text{score}_t = 0.35|z_M| + 0.30 \max(z_C, 0) + 0.25 \max(z_R, 0) + 0.10 \max(z_{\Delta M}, 0). \quad (19)$$

A light Gaussian smoothing is applied to reduce jitter. We finally apply hysteresis thresholding with high and low thresholds (`score_hi`, `score_lo`) to detect cut points, reducing false positives from noise. Segments are then assembled as:

$$[0, i_1], [i_1 + 1, i_2], \dots, [i_k + 1, n - 1].$$

**Complexity.** The dominant cost is optical flow estimation for  $n - 1$  frame pairs, while memory overhead is minimal. The method is CPU-friendly and robust to noise, making it suitable for large-scale video analysis.

## C.2 DETAILS OF SLIDING-WINDOW DETECTION

The sliding-window detection module aims to determine both the grouping and the relative position of a given video segment within the entire generated video. Leveraging the detection capability of the GF-PRC scheme, we achieve this goal efficiently. Given a video segment  $\text{VF}[t : t + l]$ , we first pad the segment with  $(c_t - 1)$  frames at the beginning, where  $c_t$  denotes the temporal compression ratio of the causal 3D VAE (e.g.,  $c_t = 4$ ). We then apply a sliding window of size  $2 \times c_t$  (e.g., 8) over the padded sequence. For each window index  $j$ , we perform inversion to obtain the local inverted initial noise:

$$z'_\tau[j : j + 1] = E_{3D}(\text{VF}'_r[j : j + 2 \times c_t]), \quad (20)$$

$$z'_0[j : j + 1] = \text{Inversion}(\mathcal{M}; z'_\tau[j : j + 1]; \text{prompt}_\theta). \quad (21)$$

Next, we use the GF-PRC keys to detect whether  $z'_0[j : j + 1]$  matches any global frame index using Eq. (6) from the main paper. This approach is effective because PRC detection accuracy is significantly higher than PRC decoding, as discussed in Section E. We also observe that repeating the same frame  $c_t$  times yields high inversion and detection accuracy, enabling the padding strategy to function correctly within the sliding window. The sliding process terminates once the detected indices form a continuous sequence, as described in the main paper. The computational complexity of this procedure is at most  $O(f \times c_t)$  and at least  $O(f)$ , which remains constant with respect to the overall generation scale.

## D ADDITIONAL EXPERIMENTAL RESULTS

### D.1 OUR CONSTRUCTED PROMPT SET

To comprehensively assess both video quality and the efficiency of the watermarking framework, we adopt VBench-2.0 (Zheng et al., 2025), a benchmark specifically designed for modern video diffusion models with stronger ability. VBench-2.0 evaluates 18 dimensions, including: Camera Motion, Complex Landscape, Complex Plot, Composition, Diversity, Dynamic Attribute, Dynamic Spatial Relationship, Human Anatomy, Human Clothes, Human Identity, Human Interaction, Instance Preservation, Material, Mechanics, Motion Order Understanding, Motion Rationality, Multi-view Consistency, and Thermotics.

We use the augmented text prompts curated for HunyuanVideo and other advanced video diffusion models. Compared to VBench-1.0 used by VideoShield (Hu et al., 2025a), our selected prompt set is more comprehensive, featuring longer and more complex descriptions that better evaluate generative capability. In total, we select 88 text prompts and generate 400 videos for each diffusion model under evaluation. For image-to-video tasks, we employ FLUX-1.0 (Black Forest Labs et al., 2025) to generate image prompts. Examples of text prompts and images used in our experiments are shown in Table 1. The full dataset will be released publicly.

### D.2 RESULTS ON WAN-2.2

To further evaluate our approach, we performed additional experiments on the Image-to-Video (I2V) and Text-to-Video (T2V) variants of the Wan-2.2 model. The results demonstrate the significant effectiveness of our method, especially showcasing superior accuracy on the I2V model. We have meticulously recorded the performance across 18 distinct prompt dimensions, with the detailed outcomes presented in Table 2.

## E PERFORMANCE BOTTLENECK AND FUTURE WORKS

Watermarking methods such as VideoShield (Hu et al., 2025a) report nearly 100% bit accuracy, but they are non-blind and incur high extraction costs at scale. In contrast, our method achieves high, though not perfect, extraction accuracy. We attribute this gap to two factors: (1) the imperfect inversion of video diffusion models and (2) the limited error-tolerance of PRC coding.

Figure 1 illustrates the relationship between inversion error and the error-tolerance characteristics of PRC. While PRC introduces diversity by encoding messages into pseudorandom sequences, this

Table 1: Our constructed prompt set – Sample of 5 dimensions with representative prompts

Dimension	Prompt Text	Image
<b>Complex Plot</b>	<p>The race commenced with explosive energy as the first runner from Team A surged ahead, capturing the attention of all spectators. His swift pace set the tone, but during the baton exchange, a slight fumble nearly cost them. Despite the near mishap, he managed to hand off the baton to the second runner, who, with fierce determination, pursued Team B relentlessly, overtaking them on the curve. However, the earlier error meant their lead was slim. As the third runner took over, nerves were palpable, yet he maintained their position, though Team C’s strategic pacing brought them dangerously close. In the final handoff, the pressure was immense. The last runner from Team A accelerated on the penultimate turn, unleashing a powerful sprint that widened the gap. With unwavering focus, he crossed the finish line triumphantly, securing victory for Team A amidst roaring cheers.</p>	
<b>Composition</b>	<p>A magnificent lion, its golden mane flowing like a regal crown, possesses the expansive, powerful wings of an eagle, each feather shimmering under the sun’s radiant glow. It soars effortlessly through a vast, azure sky, the clouds parting gracefully in its wake. The lion’s eyes, sharp and focused, scan the horizon with a kingly gaze, while its muscular body glides with the grace of a seasoned aviator. Below, the earth stretches out in a patchwork of greens and browns, rivers glistening like silver ribbons. The scene captures a breathtaking blend of strength and elegance, as the majestic creature commands the heavens with unparalleled ease.</p>	
<b>Dynamic Attribute</b>	<p>In a serene forest, the camera captures a mesmerizing transformation as vibrant red leaves slowly transition to lush green. The scene begins with a close-up of a single leaf, its deep crimson hue glowing under the gentle sunlight. As the camera pans out, the surrounding foliage reveals a tapestry of red, orange, and yellow, creating a warm, autumnal atmosphere. Gradually, the colors shift, with hints of green emerging, symbolizing the renewal of life. The sunlight filters through the canopy, casting dappled shadows on the forest floor, while a gentle breeze rustles the leaves, enhancing the sense of change and rebirth.</p>	
<b>Dynamic Spatial Relationship</b>	<p>A playful dog, with its fur slightly ruffled by the breeze, stands on the left side of a wooden dining table, its ears perked up and eyes full of curiosity. The table is surrounded by cozy chairs and a vase with fresh flowers on top. As the dog gets excited, it begins to sprint energetically towards the front of the table, its paws making soft thudding sounds against the wooden floor, eager to reach the other side where a chew toy lies waiting.</p>	
<b>Instance Preservation</b>	<p>A vibrant orange dog, with a sleek coat and playful demeanor, sprints joyfully across a sunlit meadow, its ears flapping in the breeze. The dog’s eyes sparkle with excitement as it bounds over the lush green grass, leaving a trail of paw prints behind. In the background, wildflowers sway gently, adding bursts of color to the scene. The sun casts a warm glow, highlighting the dog’s energetic movements and the natural beauty surrounding it. As the dog runs, its tail wags enthusiastically, embodying pure joy and freedom in the open, expansive landscape.</p>	

design compromises its robustness to bit flips. In Figure 1, we plot PRC detection and decoding accuracy (Y-axis) under varying bit-flip rates (X-axis). When the error rate exceeds a certain threshold, PRC decoding accuracy drops sharply toward 0.5 (random guessing). Moreover, as the encoded message length increases, this threshold becomes lower.

Table 2: Results of different models across different dimensions

Dimension	Hunyuan-I2V	Hunyuan-T2V	Wan-I2V	Wan-T2V
complex plot	1.0000	0.9292	1.0000	1.0000
composition	1.0000	0.9313	1.0000	1.0000
dynamic attribute	1.0000	0.8878	1.0000	0.8974
dynamic spatial relationship	0.9773	0.9991	1.0000	0.9554
instance preservation	0.9117	0.9584	1.0000	0.9150
motion rationality	0.9684	1.0000	1.0000	0.9379
multi-view consistency	0.9617	0.9707	0.9500	0.8820
camera motion	0.9560	0.9373	1.0000	1.0000
complex landscape	0.9913	1.0000	1.0000	1.0000
diversity	1.0000	0.9794	1.0000	0.9695
human anatomy	0.9594	0.9787	1.0000	1.0000
human clothes	0.9879	0.9927	1.0000	0.9744
human identity	0.9969	0.9304	1.0000	0.9403
human interaction	1.0000	1.0000	1.0000	0.8864
material	1.0000	0.9738	1.0000	0.8966
mechanics	0.9684	0.9377	1.0000	1.0000
motion order understanding	0.9819	0.9617	1.0000	1.0000
thermotics	0.9972	0.8815	0.9500	0.9360
Mean acc	0.9810	0.9583	0.9944	0.9550

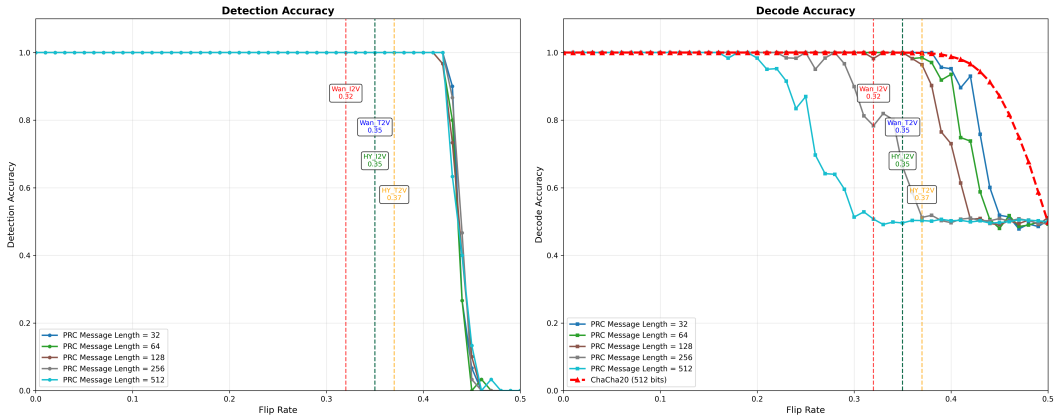


Figure 1: PRC error-tolerance curve and the inversion accuracy of different video diffusion models.

Inversion accuracy for current video diffusion models is far from perfect: HunyuanVideo exhibits an error rate of approximately 0.35, while Wan-2.2 performs slightly better at 0.32. When inversion error surpasses PRC’s tolerance, decoding becomes effectively random. In contrast, ChaCha20 combined with majority voting (red curve in Figure 1) demonstrates strong error resilience, which explains why non-blind methods like VideoShield achieve near-perfect extraction accuracy.

Fortunately, while PRC.decode() has limited fault tolerance capability, PRC.detect() exhibits strong robustness and has the potential to deliver reliable watermarking under extreme disturbances. We conduct experiments to test the false-positive rate of our proposed SIGMark, feeding the T2V generated videos into I2V model and PRC keys. The results show that 100% of the false-positive samples are distinguished as not generated by I2V model, demonstrating that our method provide reliable watermarking.

Looking forward, we identify two promising directions to improve PRC-based blind watermarking: (1) enhancing inversion accuracy through improved video inversion techniques, and (2) introducing an additional error-correcting layer on top of PRC to mitigate inversion errors.

## F USAGE OF LARGE LANGUAGE MODELS

This paper utilize Large Language Models (GPT-5) to aid the grammar mistakes and polish writing and formula, and it also helps in dealing with formatting issues during writing in  $\LaTeX$ . We also use LLM-assisted coding systems in designing and implementing experiments.

### REFERENCES

- Daniel J Bernstein et al. Chacha, a variant of salsa20. In *Workshop record of SASC*, volume 8, pp. 3–5. Lausanne, Switzerland, 2008.
- Black Forest Labs et al. Flux.1 kontext: Flow matching for in-context image generation and editing in latent space, 2025. arXiv preprint arXiv:2506.15742.
- Miranda Christ and Sam Gunn. Pseudorandom error-correcting codes. In *Annual International Cryptology Conference*, pp. 325–347. Springer, 2024.
- Runyi Hu, Jie Zhang, Yiming Li, Jiwei Li, Qing Guo, Han Qiu, and Tianwei Zhang. Videoshield: Regulating diffusion-based video generation models via watermarking. In *Proceedings of the Thirteenth International Conference on Learning Representations*, 2025a. URL <https://openreview.net/forum?id=uzz3qAYy0D>.
- Xuming Hu, Hanqian Li, Jungang Li, and Aiwei Liu. Videomark: A distortion-free robust watermarking framework for video diffusion models, 2025b.
- Jonas Thietke, Andreas Müller, Denis Lukovnikov, Asja Fischer, and Erwin Quiring. Towards a correct usage of cryptography in semantic watermarks for diffusion models. In *The 1st Workshop on GenAI Watermarking*, 2025.
- Dian Zheng, Ziqi Huang, Hongbo Liu, Kai Zou, Yinan He, Fan Zhang, Lulu Gu, Yuanhan Zhang, Jingwen He, Wei-Shi Zheng, Yu Qiao, and Ziwei Liu. Vbench-2.0: Advancing video generation benchmark suite for intrinsic faithfulness, 2025.